

Microimaging at 14 Tesla Using GESEPI for Removal of Magnetic Susceptibility Artifacts in T_2^* -Weighted Image Contrast

Qing X. Yang,^{*1} Michael B. Smith,^{*†} Richard W. Briggs,[‡] and Robert E. Rycyna[§]

^{*}Department of Radiology (Center for NMR Research) and [†]Department of Cellular and Molecular Physiology, The Pennsylvania State University, College of Medicine, The Milton S. Hershey Medical Center, Hershey, Pennsylvania 17033-2390; [‡]Departments of Radiology, Chemistry, and Biochemistry and Molecular Biology, University of Florida, Gainesville, Florida 32610; and [§]Bruker Instruments, Inc., 44 Manning Road, Manning Park, Billerica, Massachusetts 01821

Received December 7, 1998; revised August 2, 1999

In magnetic resonance imaging (MRI), T_2^* -weighted contrast is significantly enhanced by extremely high magnetic field strength, offering broad potential applications. However, the T_2^* -weighted image contrast distortion and signal loss artifact arising from discontinuities of magnetic susceptibility within and around the sample are also increased, limiting utilization of high field systems for T_2^* -weighted contrast applications. Due to the B_0 dependence of the contrast distortions and signal losses, and the heterogeneity of magnetic susceptibility in biological samples, magnetic susceptibility artifacts worsen dramatically for *in vivo* microimaging at higher fields. Practical applications of T_2^* -sensitive techniques enhanced by higher magnetic fields are therefore challenged. This report shows that magnetic susceptibility artifacts dominate T_2^* -weighted image contrast at 14 T, and demonstrates that the GESEPI (gradient echo slice excitation profile imaging) technique effectively reduces or eliminates these artifacts at long TE in the highest field (14 T) currently available for ¹H imaging. © 1999

Academic Press

Key Words: image artifacts; gradient echo; T_2^* contrast; high field MRI.

INTRODUCTION

Because of the useful information provided, T_2 - and T_2^* -weighted contrast are utilized extensively in NMR imaging. Standard T_2 -weighted sequences, however, are extremely time consuming, and the increased radio frequency (RF) power demand in conductive samples ($I-2$) severely limits the use of fast spin-echo sequences with increased RF duty cycles, especially for *in vivo* imaging at high field. As a result, gradient echo sequences have become increasingly popular, providing rapid imaging with T_2^* contrast. Spatial and temporal variations of magnetic susceptibility in living tissue that occur with certain functional, physiological, and pathological processes produce a unique image contrast in T_2^* -weighted MRI images

that can be used to study biological function. A well-known example is functional magnetic resonance imaging (fMRI) based upon the BOLD (blood oxygen level dependent) effect, which has become an important tool in brain research.

Unfortunately, contrast distortion and signal loss arising from discontinuities of magnetic susceptibility at interfaces within and around the sample are serious problems in T_2^* -weighted magnetic resonance imaging ($3-11$), especially for clinical applications and MR microscopy at high field. Since the strengths and relative extents of the local field gradients increase with B_0 field strength, the contrast distortion and signal loss artifacts worsen dramatically at higher fields for microimaging of biological samples with heterogeneous and discontinuous magnetic susceptibility distributions. This makes practical applications of T_2^* -sensitive techniques enhanced by higher magnetic fields difficult.

The effective utility of T_2^* -weighted contrast for microimaging has been limited by two major problems: (a) magnetic field inhomogeneity artifacts and (b) low contrast to noise ratio (CNR).

Imperfect static magnetic field adjustments (shimming), variations of field due to regions of differing magnetic susceptibility in tissue, and large, nonlinear local field gradients near the tissue and air interface surrounding air-containing structures inside animals and plants all produce magnetic field inhomogeneity. Such field inhomogeneity alters the T_2^* -weighted image signal and degrades the reproducibility and consistency of T_2^* contrast. By way of example, severe signal intensity loss in T_2^* -weighted images occurs in the inferior temporal rodent brain regions, adjacent to nasal, oral, sinus, and ear cavities, diminishing the usefulness of T_2^* -weighted images in these areas.

In MRI microimaging, increased spatial resolution is achieved at the cost of decreased signal-to-noise ratio resulting from the smaller voxel size. This can be recovered to some extent by signal averaging, but temporal restrictions imposed by imaging living objects make this an inefficient and often

¹ Address correspondence to Qing X. Yang, Ph.D., The Department of Radiology (Center for NMR Research), Penn State College of Medicine, 500 University Dr., Hershey, PA 17033-2390. E-mail: qing@nmr.hmc.psghs.edu.



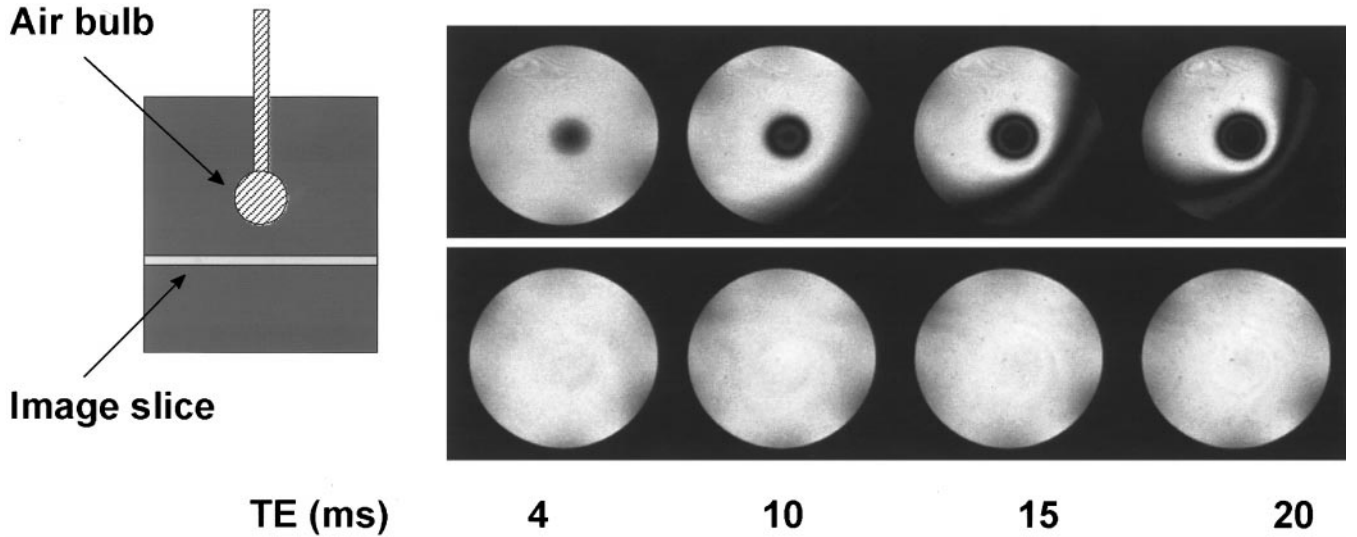


FIG. 1. Images of a gel phantom obtained from a 1-mm thick slice 1-mm from a 4-mm air-filled glass sphere. GRE (top) and GESEPI (bottom) images are shown for ascending TE values. Inset shows sphere and slice position.

impractical means of increasing signal-to-noise. Thus, it is desirable and often necessary to perform such studies at high fields. Unfortunately, while high magnetic field strengths increase the image SNR and enhance the contrast derived from tissue magnetic susceptibility, the utility of T_2^* images has been limited by artifacts which are more pronounced at high fields (7–11). Since the magnetic field inhomogeneity artifacts and the susceptibility contrast arise from a common physical mechanism, it has proved difficult to enhance the susceptibility contrast without concomitantly increasing the artifacts, or to reduce the artifacts without reducing the desired contrast.

Field inhomogeneity artifacts have been the subjects of extensive studies, some quantifying the effects (3–11) and others documenting progress toward reducing the artifacts (12–18). Cho and Ro (12) demonstrated that at a cost of a lower signal to noise ratio (SNR), signals from the homogeneous region and regions with specific static field gradients could be acquired simultaneously using a tailored excitation pulse, and they demonstrated how the susceptibility could be mapped (13). Others have shown that intravoxel dephasing artifacts are reduced in three-dimensional gradient-echo (3D-GE) images (14, 15). Field inhomogeneities can be imaged and the signal loss due to linear static field gradients of a known specific magnitude can be partially recovered by adjusting the slice refocusing gradient as suggested by Frahm *et al.* (16, 17) and extended by Ordidge *et al.* (18). The recent development of the gradient-echo slice excitation profile imaging (GESEPI) and its related multi-echo implementation multi-gradient echo with susceptibility inhomogeneity compensation (MGESIC) for recovering the signal lost due to intravoxel phase dispersion in T_2^* -weighted imaging offers a solution to this dilemma (19–21). In this report, we demonstrate that at 14 T, the usefulness of gradient-echo images is limited by the dominating magnetic

susceptibility artifacts, even at quite short TE values, and that GESEPI is effective in removing these artifacts even for TE times of 20 ms or longer. Preliminary reports of this work have been presented at several meetings (22–24).

RESULTS AND DISCUSSION

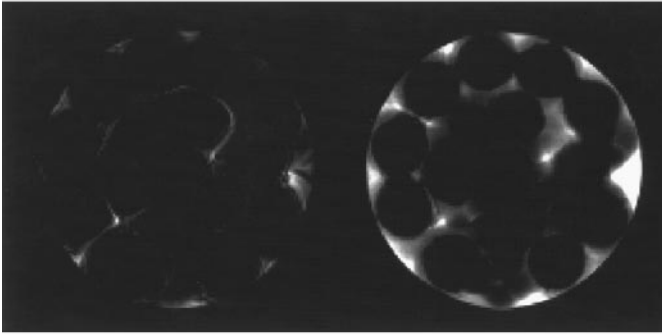
Figure 1 shows images obtained in a plane 1 mm from a 4-mm diameter spherical glass bulb of air embedded in a gelatin phantom. The GRE images show clearly the signal loss artifacts produced by the local field gradients from the sphere as well as by misadjustment of shimming. As TE increases, these artifacts progressively expand to cover more of the image areas. The bands with weak signal intensity occurring for artifact regions in the images with long TE result from a sinc-function modulation or phase wrap by local gradient (18). The dark bands curving around the center indicate that the gradients from the air bulb and misadjustment of shimming are opposite in direction. The artifacts produced by the opposite gradients from the two sources are removed in the GESEPI image at all TE values up to 20 ms.

At high field strength, subtle susceptibility differences between intracellular organelles or between cells of animal or plant and aqueous media can create significant susceptibility artifacts which obscure the details of cellular anatomy otherwise capable of being revealed by NMR microimaging. This effect can be modeled by the cylindrical phantom containing water and 4-mm glass beads shown in Fig 2. Signal around the glass/water interface is restored with the GESEPI technique.

Figure 3 shows a GRE and a GESEPI image of mouse brain. Severe signal loss artifacts near the skull and ear canals obscure the majority of the GRE image. The remaining visible portion of the GRE image showing the center of the brain is

GRE

GESEPI



TE = 10 ms

FIG. 2. GRE (left) and GESEPI (right) images of a 25-mm diameter water-filled cylinder containing 4-mm diameter glass beads, with TE = 10 ms.

blurry, with marginal contrast between different anatomical structures. The signal losses in both superior and inferior temporal areas in the GRE image are recovered in the GESEPI image, as demonstrated at lower field strength (19–21). In the presumably homogeneous region in the brain center, the GESEPI image exhibits sharper resolution and reveals remarkable anatomical details. This striking difference in image resolution was not observed at lower field strength.

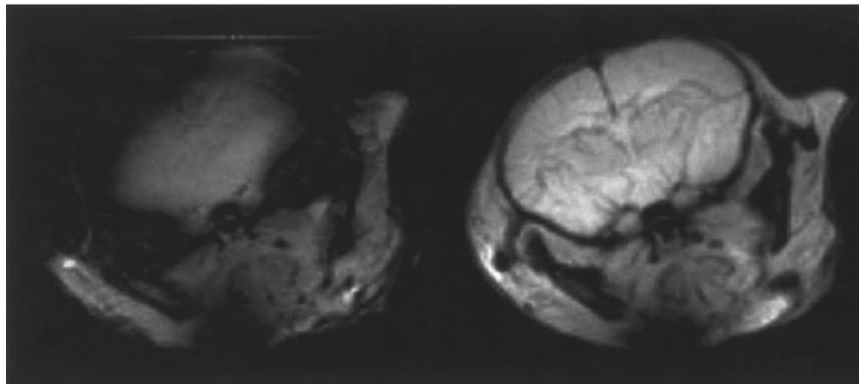
For T_2^* microimaging at 14 T, due to both higher field strength and the smaller size of the animal, the magnetic field gradients that originated at the air and tissue interfaces extend into most brain area. The magnetic susceptibility artifacts in T_2^* -weighted GRE images are no longer localized in the relatively confined areas near the air and tissue interface. The

signal intensity of the entire brain image is dictated by the macroscopic local field gradients, obscuring the desired enhancement in tissue-specific T_2^* contrast by high field strength. Signal intensities in the GESEPI images, on the other hand, are dominated by tissue-specific T_2^* contrast, exhibiting clear anatomic brain structures. This is possible because the field gradients that cause the T_2^* contrast have different physical properties than those that cause the artifacts (17, 19–21), and thus techniques can be designed to minimize image artifacts without compromising desired tissue T_2^* contrast. The field gradients that produce artifacts are macroscopic in scale, and to first approximation linear or of low-order spatial dependencies over the dimensions of the typical image voxel. The field gradients that generate the useful magnetic susceptibility based contrast, on the other hand, are microscopic in scale and vary either randomly or with high-order spatial dependence over the voxel dimensions. Therefore, it is possible for GESEPI to achieve the intended enhanced tissue-specific contrast with high field strength by removing the low-order field gradients that result in artifacts and retaining the high-order microscopic intravoxel gradients that yield a desirable contrast.

Figure 4 shows a series of GRE and GESEPI images of live adult mouse brain as a function of TE. The GRE images appear blurry, with uneven signal intensity over the image, and become progressively worse as TE increases, with increasing areas of signal void. The GESEPI images, however, provide superior image quality even at TE = 20 ms. Thus, the GESEPI technique extends the TE observation window for T_2^* contrast in very high field microimaging. This will be valuable for producing images of BOLD-based functional brain activity in small animals at high field, where the sensitivity of T_2^* mapping is significantly improved. It will also permit accurate and quantitative T_2^* measurements at high field strengths. Trans-

GRE

GESEPI



TE = 4.0 ms

TE = 6.2 ms

FIG. 3. Comparison of short TE GRE (left) and GESEPI (right) images of live mouse brain at 14 T.

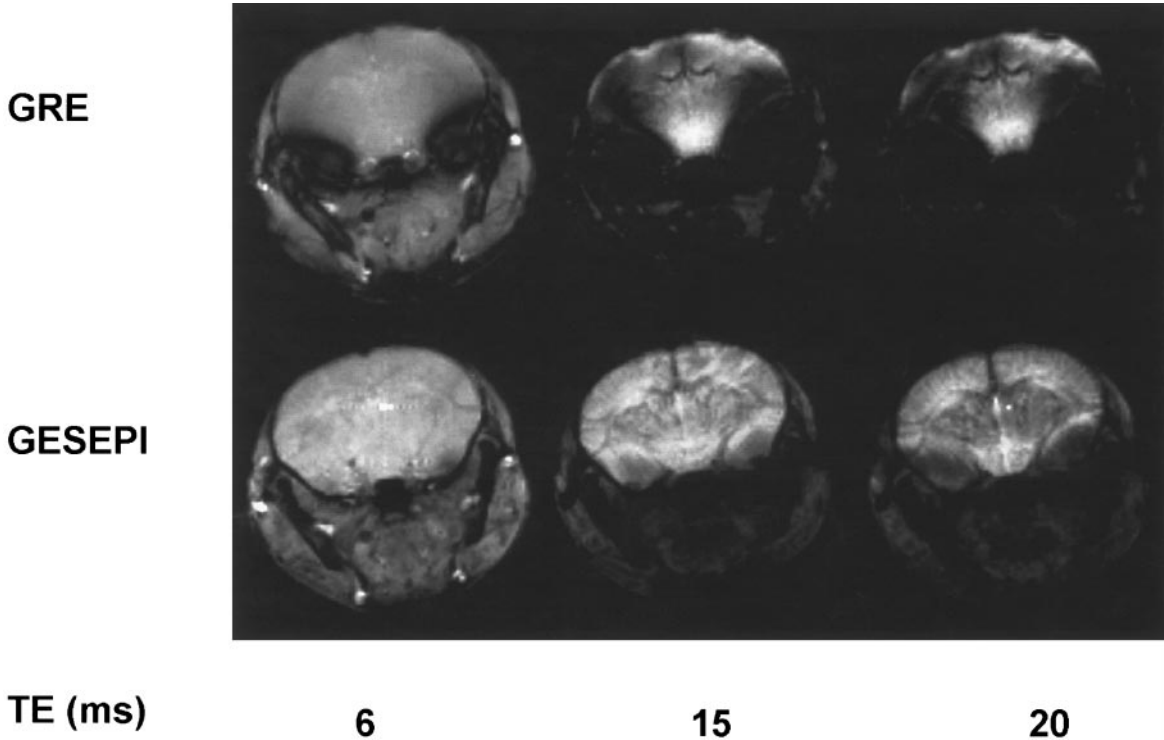


FIG. 4. *In vivo* mouse brain images obtained at 14 T with GRE (top) and GESEPI (bottom) sequences as a function of TE. TE values are 6, 15, and 20 ms (left to right).

verse relaxation follows the relationship $1/T_2^* = 1/T_2 + 1/T_2'$, where $1/T_2' = \gamma\Delta B_0/2$ is the contribution due to the local field inhomogeneity ΔB_0 . Thus this contribution, $1/T_2'$, increases linearly with field strength and can become dominant at high fields (25). For BOLD imaging of brain function and activity, the B_0^2 dependence of $1/T_2'$ found for blood (26) also contributes to the rapid T_2^* decrease in brain tissue at high field strength.

Notice that the artifacts in the GRE image at TE = 4.0 ms in Fig. 3 appear more severe than that at TE = 6.0 ms in Fig. 4. The reason is that the image in Fig. 3 has an additional local gradient on the top of the mouse's skull, causing signal loss artifacts around the cortex. The corresponding GESEPI image removed this artifact along with the artifacts around the ear canals that exist in both GRE images in Fig. 3 and 4. The problem presented here is typical for heavily T_2^* -weighted images. Because the signals in heavily T_2^* -weighted images are dominated by the local field gradient, any less than perfect shimming adjustment can alter the image contrast significantly. The heterogeneous magnetic susceptibility distribution of a biological sample makes it difficult to adjust shimming to a reproducible condition for each sample load within the allowed time frame for imaging live animals. Thus, the reproducibility and consistency of enhanced T_2^* contrast and quantitative T_2^* measurement are seriously compromised. With the aid of GESEPI, a reproducible heavily T_2^* -weighted contrast at various TE can be obtained consistently.

The tissue-specific T_2^* contrast has become increasingly important in both clinical imaging of the brain and in neurological research. For example, Ordidge *et al.* (18) have shown that quantification of T_2^* could provide a more specific assessment than T_2 of brain iron deposition, which has been implicated in several neurodegenerative diseases such as Parkinson's disease and Alzheimer's disease (27–29). Thus, with GESEPI in high fields, the enhanced T_2^* contrast allows a wide range of applications of T_2^* -weighted imaging in biomedical research.

In the GESEPI method, the incremental compensation gradient also acts as a phase-encoding gradient in the slice direction. Consequently, the excited slice is partitioned into multiple thinner slices after the third Fourier transform. Thus, GESEPI can be regarded as an over-sampled 3D method. Over-sampling here means that the FOV in slice direction is larger than the width of the excited slice. Over-sampling is necessary to remove the ghosting artifacts and compensates for the frequency shift in the slice direction (21). It is important to note that the removal of the susceptibility artifacts is not the direct result of using thinner slice thickness. The position-dependent intravoxel phase dispersion of the magnetization at TE is given by

$$\Delta\varphi = \gamma G_z^! TE \Delta z$$

where γ is the gyromagnetic ratio, $G_z^!$ is the local field gradient

along slice direction, and Δz is the slice thickness. In the GESEPI method, this phase dispersion produces an echo shift in the slice direction. For a given image plane, this echo shift can vary at different voxels because of the difference in local gradient strength, G_z^1 . The signal loss artifacts are removed as long as the echo peaks from all the voxels in the image plane are sampled by proper choice of the compensation gradient. A stronger compensation gradient is required for a larger $\Delta\phi$, which in turn leads to a thinner subslice thickness. As indicated in the equation, however, the intravoxel dispersion and the associated signal loss artifacts for conventional 2D imaging cannot be removed with the thinner slice thickness which also reduces SNR. Using thinner slice thickness with the conventional 2D method only produces a limited the artifact reduction provided TE is short and G_z^1 is relatively small.

The artifact removal with GESEPI is achieved at the expense of increased data acquisition time, which may limit its utilization in dynamic *in vivo* studies. To achieve the required temporal resolution for dynamic investigations, the GESEPI technique can be implemented with rapid imaging sequences such as spiral scanning and echo planar imaging (EPI) (30). This method offers a way to get information from areas where it otherwise would not be possible to do so, and it is more efficient than reported methods for optimizing only a single region (31, 32).

CONCLUSIONS

In summary, both phantom and *in vivo* mouse brain imaging results at 14 T demonstrate that the GESEPI method effectively reduces susceptibility artifact while retaining the enhanced T_2^* contrast at extremely high magnetic field strength. Utilization of T_2^* contrast for scientific research at high field strength can thus be exploited. The data indicate that the technique will be valuable for providing high-quality gradient echo images at long TE times with very high field, small-bore microimaging magnets. GESEPI provides a robust method of generating high T_2^* contrast images with minimal susceptibility artifacts in animals and cellular preparations at the highest imaging field strength currently available.

EXPERIMENTAL

The GESEPI sequence was implemented and the experiments were performed at the National High Magnetic Field Laboratory in Tallahassee, Florida, on an 89-mm clear-bore 14 Tesla Bruker Avance DMX-600 spectrometer (Bruker Instruments, Inc., Billerica, MA) operating at 600.2 MHz for ¹H. Imaging was done using an actively shielded gradient set and 25-mm birdcage coil.

Coronal mouse brain images at the level of the anterior ear were acquired with TR = 100 ms, FA = 25°, slice thickness = 1 mm, FOV = 20 mm, and matrix = 128 × 128 (pixel size = 156 μm). GESEPI images were acquired with 32 incremental

steps of slice refocusing gradient G_c ranging ± 250% of the normal value. Other images were acquired using similar parameters. The acquired GESEPI data set was reconstructed with a 3D complex Fourier transform, generating a set of 32 images. The final GESEPI image was obtained by adding the magnitude images within the excited slice (16 images). The remaining images in the set, containing no appreciable signal, were discarded.

A gel phantom (Knox unflavored gelatin, Nabisco, Inc., East Hanover, NJ) was prepared by pouring a 1.5-inch column into a 20-mm NMR tube. While the gel was still liquid, a 4-mm diameter air-containing glass sphere was inserted at the gel sample center.

For the *in vivo* studies, adult male Charles River Sprague–Dawley mice were anesthetized with halothane (1.5–2% for induction, 0.75–1% for maintenance) in 1.5–2:1 V:V nitrous oxide:oxygen gas at a flow rate of 600–650 cc/min. The animals were immobilized using a polysiloxane (Regisil, Dentsply International Inc., Milford, DE) mold formed between the head and a clear plastic transparency sheet rolled into a tubular holder. The anesthesia tube was fixed at the end of the holder proximal to the nose of the mouse, and the holder was placed in the NMR probe with the animal head down.

The magnetic field homogeneity was initially checked by adjusting field homogeneity on a 20-mm tube of water to a full-width half-maximum linewidth of about 20 Hz. For both phantom and animal samples, shimming was performed on the 1-mm slices used for imaging. Linewidths obtained were typically about 200 Hz.

ACKNOWLEDGMENTS

Thanks to Dr. Steve Kinsey and Dr. Steve Gibbs of the NHMFL, to Dr. Robert Werner and Linda Davis for assistance with the animals, and to Jo Ann Palmer of the NHMFL and Judy Perry of HMC for help in coordinating our visits to Tallahassee. Supported in part by the National High Magnetic Field Laboratory, the UF Brain Institute, and the Departments of Radiology of HMC and UF.

REFERENCES

1. C. H. Durney, Interactions between electromagnetic fields and biological systems, *Ann. N.Y. Acad. Sci.* **649**, 19–34 (1992).
2. P. A. Bottomley and P. B. Roemer, Homogeneous tissue model estimates of RF power deposition in human NMR studies, *Ann. N.Y. Acad. Sci.* **649**, 144–159 (1992).
3. J. F. Schenck, The role of magnetic susceptibility in magnetic resonance imaging: MRI magnetic compatibility of the first and second kinds, *Med. Phys.* **23**, 815–850 (1996).
4. C. J. G. Bakker, R. Bhagwandien, M. A. Moerland, and M. Fuderer, Susceptibility artifacts in 2DFT spin-echo and gradient-echo imaging: the cylinder model revisited, *Magn. Reson. Imaging* **11**, 539–548 (1993).
5. K. M. Ludeke, P. Roschmann, and R. Tischler, Susceptibility artifacts in NMR imaging, *Magn. Reson. Imaging* **3**, 329–343 (1985).
6. J. R. Reichenbach, R. Venkatesan, D. A. Yablonskiy, M. R. Thompson, S. Lai, and E. M. Haacke, Theory and application of static field

- inhomogeneity effects in gradient-echo imaging, *J. Magn. Reson. Imaging* **7**, 266–279 (1997).
7. S. Posse and W. P. Aue, Susceptibility artifacts in spin-echo and gradient-echo imaging, *J. Magn. Reson.* **88**, 473–492 (1990).
 8. D. A. Yablonskiy and E. M. Haacke, Theory of NMR signal behavior in magnetically inhomogeneous tissues: The static dephasing regime, *Magn. Reson. Med.* **32**, 749–763 (1994).
 9. E. M. Haacke, P. A. Wielopolski, and J. A. Tkach, A comprehensive technical review of short TR, fast, magnetic resonance imaging, *Rev. Magn. Reson. Med.* **3**, 53–170 (1991).
 10. S. Li, G. D. Williams, T. A. Frisk, B. W. Arnold, and M. B. Smith, A computer simulation of the static magnetic field distribution in the human head, *Magn. Reson. Med.* **34**, 268–275 (1995).
 11. S. Li, B. J. Dardzinski, C. M. Collins, Q. X. Yang, and M. B. Smith, Three-dimensional mapping of the static magnetic field inside the human head, *Magn. Reson. Med.* **36**, 705–714 (1996).
 12. Z. H. Cho, and Y. M. Ro, Reduction of susceptibility artifact in gradient-echo imaging, *Magn. Reson. Med.* **23**, 193–200 (1992).
 13. Y. M. Ro and Z. H. Cho, Susceptibility magnetic resonance imaging using spectral decomposition, *Magn. Reson. Med.* **33**, 521–528 (1996).
 14. E. M. Haacke, J. A. Tkach, and T. B. Parrish, Reduction of T_2^* dephasing in gradient field echo imaging, *Radiology* **170**, 457–462 (1989).
 15. J. Ma, F. W. Wehrli, and H. K. Song, Fast 3D large-angle spin-echo imaging (3D FLASE), *Magn. Reson. Med.* **35**, 903–910 (1996).
 16. J. Frahm, K. D. Merboldt, and W. Hänicke, Direct FLASH MR imaging of magnetic field inhomogeneities by gradient compensation, *Magn. Reson. Med.* **6**, 474–480 (1988).
 17. J. Frahm, K.-D. Merboldt, and W. Hänicke, The effects of intravoxel dephasing and incomplete slice refocusing on susceptibility contrast in gradient-echo MRI, *J. Magn. Reson. Series B* **109**, 234–237 (1995).
 18. R. J. Ordidge, J. M. Gorell, J. C. Deniau, R. A. Knight, and J. A. Helpert, Assessment of relative brain iron concentrations using T2-weighted and T_2^* -weighted MRI at 3.0 Tesla, *Magn. Reson. Med.* **32**, 335–41 (1994).
 19. Q. X. Yang, B. J. Dardzinski, G. D. Williams, and M. B. Smith, Magnetic susceptibility contrast using an imbalanced slice refocusing gradient: a gradient-echo method for high field MRI, in "Proc. ISMRM, 4th Ann. Meeting, New York, 1996," p. 1676.
 20. Q. X. Yang, B. J. Dardzinski, S. Li, and M. B. Smith, Multi-gradient echo with susceptibility inhomogeneity compensation (MGESIC): Demonstration of fMRI in the olfactory cortex at 3.0 T, *Magn. Reson. Med.* **37**, 331–335 (1997).
 21. Q. X. Yang, G. D. Williams, R. J. Demeure, T. J. Mosher, and M. B. Smith, Removal of local field gradient artifacts in T_2^* -weighted images at high fields by gradient-echo slice excitation profile imaging, *Magn. Reson. Med.* **39**, 402–409 (1998).
 22. Q. X. Yang, G. D. Williams, R. J. Demeure, R. W. Briggs, and M. B. Smith, Removal of local field gradient artifacts in T_2^* -weighted images in high field, in "38th Experimental Nuclear Magnetic Resonance Conference (ENC), Orlando, Florida, March 23–27, 1997," abstract P-011.
 23. Q. X. Yang, B. J. Dardzinski, R. J. Demeure, R. W. Briggs, and M. B. Smith, Removal of local field gradient artifacts in T_2^* measurement and T_2^* contrast at high field, in "Proc. 6th ISMRM, 1998," Vol. 1, p. 578.
 24. Q. X. Yang, R. W. Briggs, and M. B. Smith, T_2^* -weighted microimaging at 14 Tesla with the GESEPI method for removal of magnetic susceptibility distortion, in "Proc. 6th ISMRM, 1998," Vol. 1, p. 407.
 25. H. K. Song, F. W. Wehrli, and J. Ma, Field strength and angle dependence of trabecular bone marrow transverse relaxation in the calcaneus, *J. Magn. Reson. Imaging* **7**, 382–388 (1997).
 26. K. R. Thulborn, J. C. Waterton, P. M. Matthews, and G. K. Radda, Oxygenation dependence of the transverse relaxation time of water protons in whole blood at high field, *Biochim. Biophys. Acta* **714**, 265–270 (1982).
 27. S. M. LeVine, Iron deposition in multiple sclerosis and Alzheimer's disease brains, *Brain Res.* **760**, 298–303 (1997).
 28. M. A. Deibel, W. D. Ehmann, and W. R. Markesbery, Copper, iron, and zinc imbalance in severely degenerated brain regions in Alzheimer's disease: Possible relation to oxidative stress, *J. Neurol. Sci.* **143**, 137–142 (1996).
 29. R. J. Conner, A quantitative analysis of isoferitins in select regions of aged, Parkinsonian, and Alzheimer's diseased brains, *J. Neurochem.* **65**, 717–724 (1995).
 30. Q. X. Yang, W. B. Edmister, K. K. Kwong, R. J. Demeure and M. B. Smith, Removal of the signal loss artifacts in T_2^* -weighted EPI, in "Proc. 6th ISMRM, 1998," Vol. 1, p. 1443.
 31. G. H. Glover and S. Lai, Reduction of susceptibility effects in BOLD fMRI using tailored RF pulses, in "Proc. 6th ISMRM, 1998," Vol. 1, p. 298.
 32. D. Cordes, P. A. Turski, and J. A. Sorenson, Automated signal recovery of signal void arising from static field inhomogeneities in echoplanar imaging by z-gradient refocusing, in "Proc. 6th ISMRM, 1998," Vol. 1, p. 417.